Experimental integration of a 4-level primitive equation model of the atmosphere

By HANS ØKLAND, *Norwegian Meteorological Institute, Oslo, Norway*

(Manuscript received August 26, 1968, revised version December 3, 1968)

ABSTRACT

A numerical weather prediction model is presented. Care has been taken to select the reference levels in such a way that a good description of the vertical structure of the atmosphere is obtained. An experimental integration is performed, starting with a small perturbation superimposed on a linear baroclinic flow. The results are analyzed and discussed, with special emphasis on the frontogenetic processes.

Introduction

The experiment to be described in the following, is intended to be a study of the frontogenetic processes in a deepening cyclone. The vertical circulations associated with these processes are not easily observed in the atmosphere, but readily computed from the results of the integration. We have wanted to keep the experiment as simple as possible, and therefore latent heat and mixing processes are kept out of consideration. Also, in order to reduce the amount of computations involved, an attempt has been made to select the reference levels in the model in such a way that an optimal description of the vertical structure of the atmosphere is obtained.

Obviously, a numerical model based on this last principle has a great advantage in weather prediction, where the question of economy is crucial. Therefore, to test the stability and general behaviour of such a model has been the second objective of the experiment.

Proceeding now to a discussion of how to select the reference levels, the first thing to be considered is the question of how good a resolution we want in the vertical direction. There may be special need for a very accurate description of certain elements. For instance, a high resolution of the static stability may be necessary in order to forecast cloud tops. We shall here, however, ask the more general question about the necessary vertical resolution in order to forecast correctly the large scale atmospheric phenomena. We admit that we do not know the answer to this question, but believe that some information can be drawn from what is known about the statistics and dynamics of the atmosphere. We know, for instance, that the horizontal wind speed has its maximum value close to the tropopause. A sufficiently accurate description of the height and intensity of this maximum is necessary in order to describe the kinetic energy of the atmosphere. Furthermore, since there is an abrupt change at the tropopause in the static stability, and since the latter plays an important role not only for convective phenomena, but also for baroclinic instability and cyclone development, one should think that the height of the tropopause is of importance also in this connection. This leads to the conclusion that if we want the number of reference levels to be small, the tropopause should be chosen as one such level, where both the horizontal wind and the temperature are given.

This idea is not a new one. Several models have been proposed or used, which carry the tropopause as a co-ordinate surface (see for instance Shuman & Hovermale, 1968). The question then arises about how to treat this surface in the model. Certainly it should not be considered as an isobaric surface, because of the considerable variation in the height of the tropopause in time and in horizontal direction. There is little doubt, however, that over a short time period the tropopause can be considered as a material surface. On the other hand we know that there are mixing processes across the tropopause, and that radiation acts efficiently to destroy existing tropopauses and create new ones. However, we shall leave these processes out of consideration, and restrict the integration to a time period which is short enough to allow us to treat the tropopause as a material surface.

Analyses of the upper atmosphere indicate that the tropopause tends to coincide with an isentropic surface (Newton & Person, 1962), although different sheets of the tropopause coincide with different isentropic surfaces. This has been utilized in tropopause analysis (Gustafson, 1965). We shall here simply assume that there is only one tropopause, which coincides with an isentropic surface. However, in an operational model to be used for an extended horizontal area, two or more isentropic levels could be used, each of which coincides with a sheet of the tropopause.

A static stability in the troposphere may now be defined by choosing the earth's surface as a co-ordinate surface for the temperature. This surface will also be a material one. The static stability in the lowest 2000–3000 m of the troposphere frequently is much different from the stability in the upper part of the troposphere (Nordø, 1965). Therefore, the 700 mb surface is chosen as an additional co-ordinate level for the temperature. The wind will be given in both these two lowest levels. This is not necessary, but makes the model more simple.

We also want to describe the mean static stability in the stratosphere, and for that purpose the temperature in one more level in the upper part of the stratosphere is needed. In the experiment the 50 mb surface is used. Here, too, we shall have the velocity components given, and also assume that ω, the vertical velocity in pressure co-ordinates, is zero. This makes also the top level a material surface.

The differential equations

The co-ordinate levels will be indicated by the numbers 0, 1, 2 and 3 from top to bottom. A variable will be given a subscript to indicate the level to which it belongs. The letter k will be used to indicate an arbitrary level.

Independent variables are x, y and t. We shall distinguish between two kinds of dependent variables: the prognostic and the diagnostic ones. The prognostic variables, which carry the history of the computations, are computed from the prognostic equations. These variables are the horizontal velocity, $\mathbf{v}$, in all levels, the potential temperature, θ, in the levels 0, 2 and 3, and the pressure, p, in the levels 1 and 3. The diagnostic variables are derived from the prognostic variables by means of the diagnostic relations. These variables are: the Exner function, $\pi = (p/100)^{0.286}$, in the levels 1 and 3, the geopotential, ϕ, in the levels 0, 1 and 2, the Montgomery potential, $M = \phi + c_p \theta \pi$, in the level 1, and finally $\omega = dp/dt$ in level 2.

We shall use the abbreviations

$$\mathbf{A}_k = \mathbf{v}_k \cdot \nabla \mathbf{v}_k + \mathbf{k} \times f \mathbf{v}_k$$

$$H_k = \mathbf{v}_k \cdot \nabla \theta_k$$

$$D_k = \tfrac{1}{2} \nabla \cdot [(p_k - p_{k-1})(\mathbf{v}_k + \mathbf{v}_{k-1})]$$

$$G_k = \tfrac{1}{2} c_p (\theta_k + \theta_{k+1})(\pi_{k+1} - \pi_k),$$

where ∇ is the horizontal Nabla operator, taken in the co-ordinate surface where the variable is defined.

The prognostic equations for the horizontal velocity may then be written as

$$\frac{\partial \mathbf{v}_0}{\partial t} = -\mathbf{A}_0 - \nabla \phi_0$$

$$\frac{\partial \mathbf{v}_1}{\partial t} = -\mathbf{A}_1 - \nabla M_1$$

$$\frac{\partial \mathbf{v}_2}{\partial t} = -\mathbf{A}_2 - \omega_2 (\mathbf{v}_3 - \mathbf{v}_1)/(p_3 - p_1) - \nabla \phi_2$$

$$\frac{\partial \mathbf{v}_3}{\partial t} = -\mathbf{A}_3 - c_p \theta_3 \nabla \pi_3.$$

These equations are recognized as the equations of motion. The Coriolis parameter, f, is assumed to be a constant equal to 10^{-4} sec^{-1}. The earth's surface is assumed to be flat.

The first law of thermodynamics gives the prognostic equations for the potential temperature. Assuming an adiabatic atmosphere we get

$$\frac{\partial \theta_0}{\partial t} = -H_0$$

$$\frac{\partial \theta_2}{\partial t} = -H_2 - \omega_2 (\theta_3 - \theta_1)/(p_3 - p_1)$$

$$\frac{\partial \theta_3}{\partial t} = -H_3.$$

The last two prognostic equations are derived from the equation of continuity, integrated downwards from the top level where the pressure is constant. They are

$$\frac{\partial p_1}{\partial t} = -D_1$$

$$\frac{\partial p_3}{\partial t} = -D_1 - D_2 - D_3.$$

Two of the diagnostic relations are already given, namely the definition equations for π and M. There remain 4:

$$\omega_2 = -D_1 - D_2$$

$$\phi_2 = G_2$$

$$\phi_1 = G_2 + G_1$$

$$\phi_0 = G_2 + G_1 + G_0.$$

The first of these equations is derived from the equation of continuity, and the last 3 are derived from the finite difference approximation to the hydrostatic equation, integrated upwards from the ground.

Boundary condition

The domain of integration is bounded by two vertical walls parallel two the x axis, and 5100 km apart. In the x direction a cyclic condition is imposed on the dependent variables, so that they have the same value for x and $x+L$, where L is taken to be 5400 km.

Let u and v have the usual meaning as velocity components. At the walls we must have $v=0$, but we shall also assume, somewhat arbitrarily, that $\partial^2 v/\partial y^2 = \partial u/\partial y = \partial\theta/\partial y = \partial p/\partial y = 0$. These last relations are necessary in order to define all the terms in the finite difference equations on the boundaries.

Finite difference approximations

The finite difference approximations are constructed for a grid which is "staggered" in space and time, in the way described by Eliassen (1956). Let

$$\alpha_{i,j,n} \equiv \alpha(ih, jh, n\Delta t),$$

where α is a dependent variable. Then, if i, j and n are integers, the grid-point values of the different variables are

$$u_{i,j+\frac{1}{2},n}; \quad u_{i+\frac{1}{2},j,n+\frac{1}{2}}$$

$$v_{i+\frac{1}{2},j,n}; \quad v_{i,j+\frac{1}{2},n+\frac{1}{2}}$$

$$p_{i,j,n}; \quad p_{i+\frac{1}{2},j+\frac{1}{2},n+\frac{1}{2}}$$

$$\omega_{i+\frac{1}{2},j+\frac{1}{2},n}; \quad \omega_{i,j,n+\frac{1}{2}}.$$

θ, π, ϕ and M are given in the same points as p.

The derivatives are approximated by means of first order centered differences, both in the x and y direction, and in time. Where values of variables are needed, which are not defined in the appropriate grid-points, the general rule is to form a suitable mean from the nearest surrounding gridvalues. However, the advective terms in the momentum equations are written as

$$h^{-1}(\bar{u}^{xy}\delta_x \bar{u}^y + \bar{v}^{yy}\delta_y \bar{u}^x)$$

$$h^{-1}(\bar{u}^{xx}\delta_x \bar{v}^y + \bar{v}^{xy}\delta_y \bar{v}^x)$$

where a bar represents the mean operator in the direction indicated, and δ is the corresponding difference operator. These formuli are different from those given by Eliassen (1956), but they expand in a similar way to

$$\delta_x(\bar{u}^y\bar{u}^y) + \delta_y(\bar{v}^y\bar{u}^x) - \bar{u}^{xy}(\delta_x \bar{u}^y + \delta_y \bar{v}^y)$$

$$\delta_x(\bar{u}^x\bar{v}^y) + \delta_y(\bar{v}^x\bar{v}^x) - \bar{v}^{xy}(\delta_x\bar{u}^x + \delta_y \bar{v}^x).$$

Consider now the local change in u^2 and v^2 brought about by the two first terms in the last expressions above. For u^2 we get

$$\frac{h}{2}\frac{\partial}{\partial t}u^2 = hu\frac{\partial u}{\partial t} \approx \bar{u}^{xy}[\delta_x(\bar{u}^y\bar{u}^y) + \delta_y(\bar{v}^y\bar{u}^x)]$$

and a similar equation for v^2. The terms in square brackets will vanish if summed over the domain, but the whole right hand side will not, as may easily be shown. Therefore, the time derivative of the horizontally averaged variance of the velocity components does not vanish. A slightly more complicated scheme which has this property is the following

$$h^{-1}[\delta_x(\bar{u}^y\bar{u}^{xxy}) + \delta_y(\bar{v}^y\bar{u}^{xyy})]$$

$$h^{-1}[\delta_x(\bar{u}^x\bar{v}^{xxy}) + \delta_y(\bar{v}^x\bar{v}^{xyy})]$$

These formuli should presumably lead to better numerical stability (Bryan, 1966). However, in the experiment described in this paper, which was carried out to 120 hours, the first approximation gave completely stable computations. Moreover, the results showed so good continuity between the fields of the dependent variables at time-step n and $n+\frac{1}{2}$ that the two fields could be analysed simultaneously, thus effectively reducing the mesh size by a factor of $\sqrt{2}$. The separation in time, 10 minutes, between the two fields is of no significance as far as synoptic scale phenomena are concerned.

The increments used are $h = 600$ km in the x and y direction and $\Delta t = 20$ minutes in time.

Initial values

The schematic vertical cross section normal to the walls, shown on Fig. 1, demonstrates the starting condition for the integration. A baroclinic flow is constructed by means of a prescribed variation in pressure and temperature in the direction of the y co-ordinate. This variation is

$$K_1 - K_2 \sin(2\pi y/L) \quad \text{when} \quad -L/4 \leqslant y \leqslant L/4.$$
$$K_1 + K_2 \quad \text{when} \quad y < -L/4.$$
$$K_1 - K_2 \quad \text{when} \quad y > L/4.$$

The values of K_1 and K_2 for the variables in question can be read out of Fig. 1.

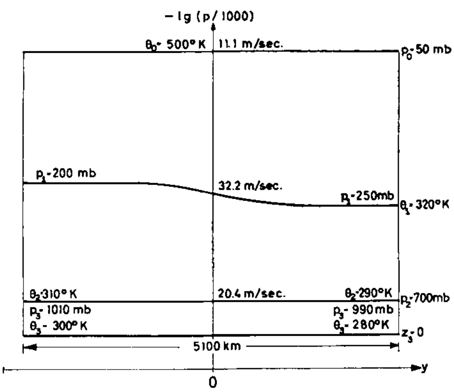

Fig. 1. Vertical cross section normal to the parallel walls which bound the horizontal domain considered, showing the reference levels, the variables, and how the baroclinic flow is constructed.

The hydrostatic equation is then integrated to get the geopotential (or the Montgomery potential), and after that the wind components are computed from the geostrophic wind formula. Note that the baroclinic flow is confined to the central part of the domain. This is done to prevent the walls from interfering too much with the development in the interior of the domain.

Superimposed on this baroclinic flow is a small perturbation in the pressure of the lowest level, prescribed as

$$5\cos(2\pi y/L)\sin(2\pi x/L) \quad \text{when} \quad |y| \leqslant L/4$$
$$0 \quad \text{when} \quad |y| > L/4.$$

Actually this perturbation is added to the surface pressure before ϕ, M, u, and v are computed. What this procedure does, is practically equivalent to adding the same wind perturbation in all levels.

Results

The computer program was coded in the "Algol" language, and run on the "Facit" computer owned by the Norwegian Meteorological Institute. The computations were discontinued when a 5 days prognosis had been computed. At that time the results were still well-behaved in the sense that no definite signs of instability or noise could be detected.

Fig. 2 shows in succession the initial values and the prognostic values after 1, 2, 3, 4 and 5 days of the surface pressure. The intitial disturbance with an amplitude of 5 mb is seen to grow rather slowly at first, but more quickly later, until after 5 days the pressure in the low center has become below 960 mb and in the high center above 1040 mb. As could be expected the disturbance is fairly close to its initial sinusoidal shape as long as it is small, that is until about 2 days. After that time the nonlinear effects become relatively more important, so that already after one more day the ansymmetric shape is noticable. Finally after 5 days a number of small-scale lows and highs have developed. Some of these small disturbances may be interpreted as for instance cold front waves, but others seem to be more unrealistic. Similar small-scale phenomena also occur in the experiments described by Edelmann (1963). Although

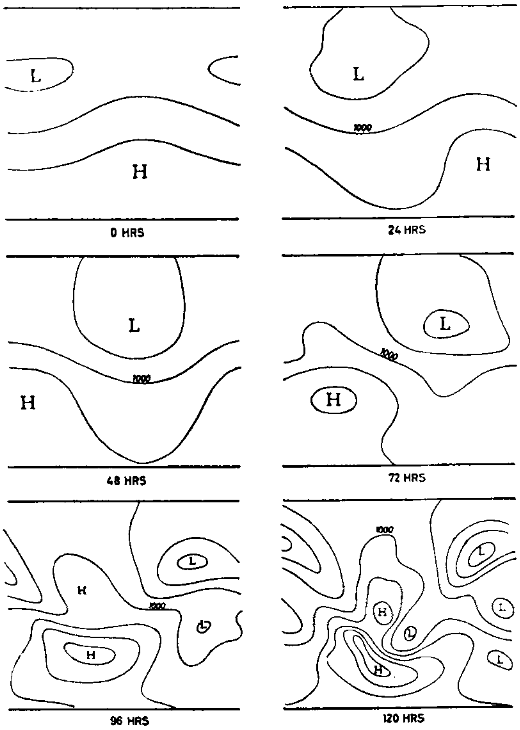

Fig. 2. Initial values and prognostic values after 1, 2, 3, 4 and 5 days of the surface pressure (p_3). Isolines are drawn at 10 mb intervals.

their structure seems to be very much the same as that of the greater cyclone which develops first, they probably are caused by a different mechanism. Whereas the initial cyclone grows from a small disturbance as a result of the baroclinic instability, the "second generation" lows probably develop from deformations brought about by the "mother" cyclone, and these deformations need not necessarily be of small amplitude.

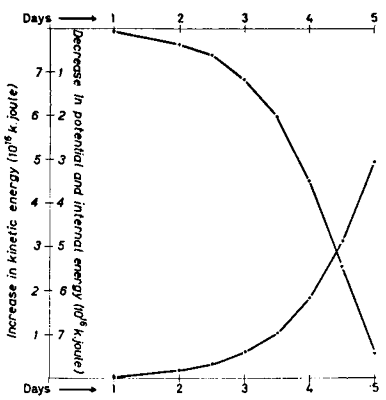

Fig. 3. Increase in kinetic energy and decrease in the sum of potential and internal energy.

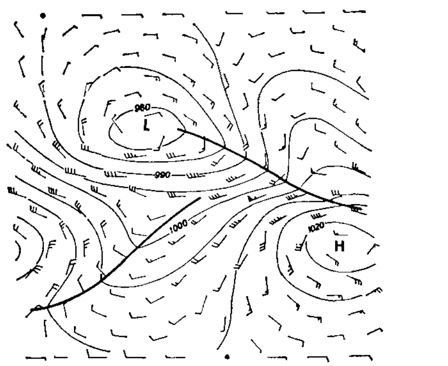

Fig. 4. Wind (v_3) and pressure (p_3) in the lowest level after 3 days (72 hrs). Isolines are drawn at 5 mb intervals.

Assuming that in experiments of this kind, small-scale cyclones and anticyclones develop more frequently than they do in nature, one may speculate about the reason for this difference. It is possible that physical effects missing in the model greatly modify these disturbances in the real atmosphere. Another possibility is that some of them are caused or initiated by integration errors. One type of such errors, which could be of importance in this respect, is observed in the temperature forcast for the lowest level (shown on Fig. 5 for the 3 days prognosis). In this level the temperature changes only by horizontal advection. Therefore no

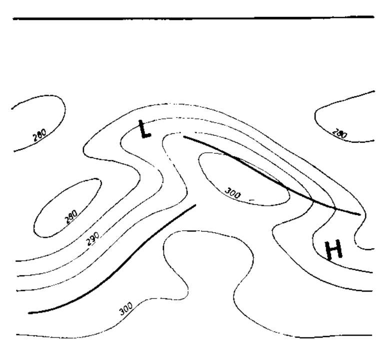

Fig. 5. Potential temperature in the lowest level (θ_3) after 72 hrs.

temperature higher than the highest temperature in the initial field should occur at any later instance. Similarly, there should be no temperature lower than the lowest in the initial data. This is not the case, however. After 3 days there has been a moderate rise of about 3° in the warm tongue, and a similar fall in the cold air. This error becomes rapidly worse later

Special numerical studies have been performed on this subject, and they indicate that the errors are associated with the strong temperature gradients which gradually develop in the lowest level, and that they show signs of a wave-like propagation. However, we shall here refrain from a further discussion on this subject.

Fig. 3 shows the increase in the kinetic energy and the decrease in the sum of potential and internal energy (in the following called potential energy for short). In each grid-point the kinetic energy is computed from

$$\frac{h^2}{4g}\sum_{k=0}^{2}(\mathbf{v}_k^2+\mathbf{v}_{k+1}^2)(p_{k+1}-p_k)$$

and the potential energy from

$$\frac{c_p h^2}{2g}\sum_{k=0}^{2}(\theta_k\pi_k+\theta_{k+1}\pi_{k+1})(p_{k+1}-p_k).$$

The values for all grid-points are then added, and the sum for the initial data is subtracted.

From the beginning and until 4 days the increase in the kinetic energy is about one half of the decrease in potential energy. Later on the decrease in potential energy becomes relatively smaller, so that from $4\frac{1}{2}$ to 5 days it about balances the increase in kinetic energy. In other words there appears to be an energy sink in the model during the first 4 days. The reason for this is not quite clear. It may be that this is caused by the finite difference scheme, and that it helps to keep the computations stable. If this is the case, the relatively large increase in the kinetic energy after 4 days could be an indication of computational instability.

In the following we shall study the results after 3 days somewhat more in detail. At that time the intial perturbation has grown into a well developed low and a corresponding high, but the secondary disturbances have just begun to show up. Fig. 4 shows the horizontal wind, plotted in the grid-points as observations on a weather map. In relation to Fig. 2 the fields have been displaced along the x-axis in order to bring the low center near the middle of the figure. In each point, values of u and v at two consecutive time-steps have been used, since u at even time-steps is given in the same points as v at odd time-steps. On the figure are also drawn isolines for the surface pressure.

The wind is obviously nearly geostrophic. This shows that the results contain the same delicate balance between wind and horizontal pressure force as the atmosphere. Another indication of this balance is that the horizontal divergence shown on the figures 8, 9 and 10 has the characteristic value 10^{-5} sec^{-1}, one order of magnitude smaller than the vorticity.

On Fig. 4 heavy lines are drawn in the sharp pressure troughs. These troughs are well defined both by the pressure and the corresponding wind field. The same trough-lines are copied on the following figures, in order to make the comparison easier. The position of the surface low and high center is also indicated, for the same reason.

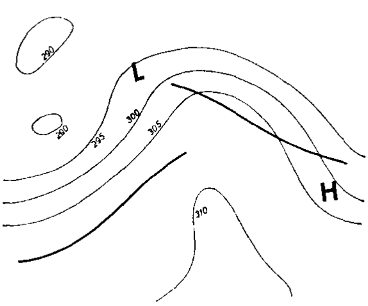

Fig. 6. Potential temperature in the 700 mb level (θ_2) after 72 hrs.

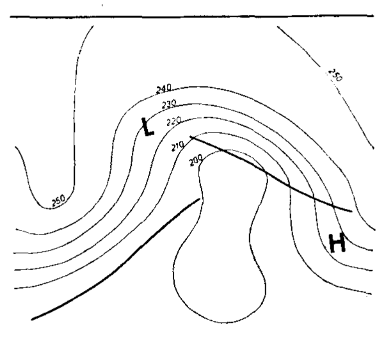

Fig. 7. Tropopause pressure (p_1) after 72 hrs.

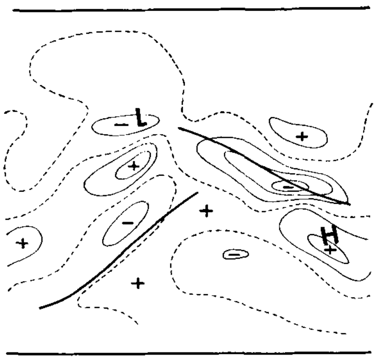

Fig. 8. Horizontal divergence in the lowest level $(\nabla \cdot v_3)$ after 72 hrs. Isolines are drawn at 5×10^{-6} sec^{-1} intervals. The zero line is broken.

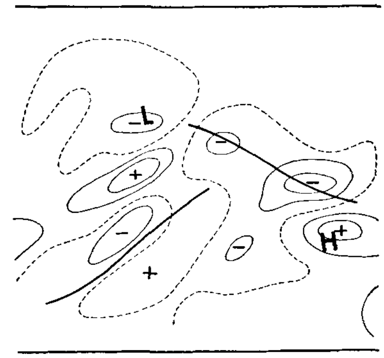

Fig. 10. Horizontal divergence in the top level $(\nabla \cdot v_0)$ after 72 hrs. Isolines are drawn at 5×10^{-6} sec^{-1} intervals.

Fig. 5 and Fig. 6 show the temperature in the two lowest levels, and Fig. 7 shows the pressure of the tropopause. Since the tropopause is an isentropic level in this experiment, the lines on Fig. 7 are closely related to the temperature in the upper troposphere and the stratosphere.

While the temperature field in the upper levels shows a smooth, meandering form, it has been highly distorted in the bottom level. In particular one should note the way the isotherms have been packed along the trough lines in the lowest level, thus creating a very realistic picture of fronts on a surface weather map. This is quite similar to the results obtained by Edelmann (1963) and Eliassen & Raustein(1967).

The mechanism which leads to this deformation of the isotherms becomes clear when looking at the horizontal divergence and the vertical velocity (Figs. 8 to 12). In the lowest level (Fig. 8) there are belts of strong convergence and divergence parallel to the "fronts". The belt of convergence is seen to be on the warmer side of the packed isotherms, while the divergence is on the colder side. The wind resulting from these fields of divergence and convergence obviously will squeeze the isotherms more tightly together. This must be the way the strong thermal gradients have developed. In fact, it can be shown by inspecting the divergence and convergence at earlier time-steps.

The convergence on the warmer side of the frontal zone will create the cyclonic vorticity associated with the wind change in the pressure trough. Since this vorticity is advected in the same wind field as the isotherms, the trough will stay in the same position relative to the isotherms, and intensify as long as there is convergence in this position. The convergence in its

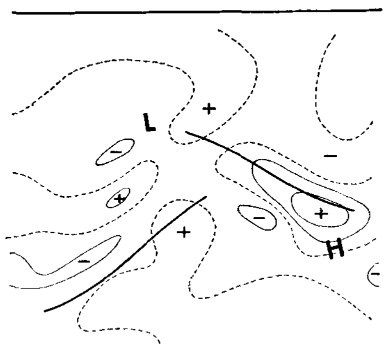

Fig. 9. Horizontal divergence in the 700 mb level $(\nabla \cdot v_2)$ after 72 hrs. Isolines are drawn at 2×10^{-6} sec^{-1} intervals.

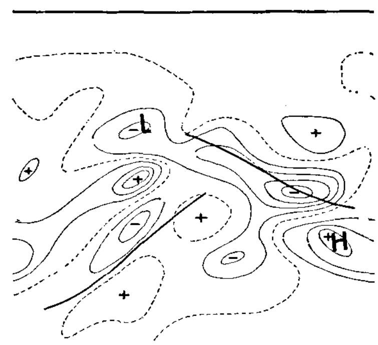

Fig. 11. Vertical velocity in pressure co-ordinates in the 700 mb level (ω_2) after 72 hrs. Isolines are drawn at 5×10^{-5} cb/sec intervals.

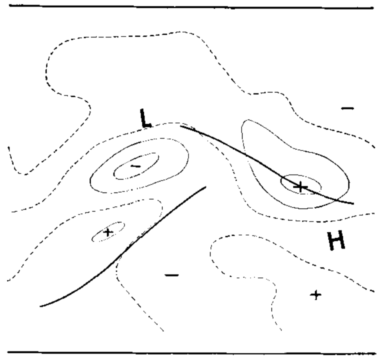

Fig. 12. Vertical velocity in pressure co-ordinates in the tropopause level (ω_1) after 72 hrs. Isolines are drawn at 2×10^{-5} cb/sec intervals.

turn is tied to the thermal zone. This can be shown by means of the quasi-geostrophic theory (see for instance Eliassen, 1966). Further, this theory predicts that the convergence will be on the warmer side of the thermal zone.

In the 700 mb level (Fig. 9) there are similar regions of divergence and convergence, but they are much weaker, about one third of the value in the lowest level (note that the isolines are drawn at different intervals in these figures). This explains why the temperature field is less distorted in the upper level than in the lower.

Turning now to the top level (Fig. 10) we find values of divergence and convergence of the same magnitude as in the bottom level. The reason for this must be that this top level, with $\omega = 0$, acts as a "lid" on the model atmosphere, and it demonstrates how the mechanism which produces the strong thermal gradients associated with fronts, is connected with the horizontal boundaries. (The reason why strong temperature gradients are not present in the top level is that the temperature there was constant initially in this experiment.)

The two last figures show the vertical velocity in the 700 mb level (Fig. 11) and in the tropopause (Fig. 12). In the tropopause the vertical velocity is not given explicitely, but can easily be computed from the other variables. As one could expect there is ascending motion at 700 mb above the region of strong convergence in the surface level. In the tropopause, however, there is a (somewhat smaller) descending motion in the same locations. Clearly we have the following vertical circulation normal to the fronts: In the troposphere there is ascending motion along the warmer side of the strong thermal fields, and descending motion along the colder side. In the stratosphere there is a (conciderably weaker) circulation in the opposite direction. This reversed circulation in the stratosphere is connected with the circumstance that the horizontal temperature gradient has opposite directions in the troposphere and in the stratosphere.

Acknowledgements

The author is indebted to Director dr. R. Fjørtoft for stimulating discussions, and to Mr. Wiggo Hårvig for help in preparing the figures.

This work was in part sponsored by U.S. Air Force Contract No. AF 61 (052)-374.

REFERENCES

Bryan, K. 1966. A scheme for numerical integration of the equation of motion on an irregular grid free of nonlinear instability. *Monthly Weather Review, 94,* No. 1, 39–40.

Edelmann, W. 1963. On the behaviour of disturbances in a baroclinic channel. *Technical Note,* German Weather Service, Research Division, Offenbach.

Eliassen, A. 1956. A procedure for numerical integration of the primitive equations of the two-parameter model of the atmosphere. *Scientific Report No. 4,* University of California at Los Angeles.

Eliassen, A. 1966. *The Cload-Forming Circulations in Fronts.* Lecture held at the Nato Advanced Study Institute on the dynamics of louds and cloud systems. University of Oslo, 1966.

Eliassen, A. & Raustein, E. 1967. A numerical integration experiment with a model atmosphere based on isentropic surfaces. *Meteorologiske Annaler,* Det Norske Meteorologiske Institutt, Oslo, *5,* No. 2, 45–63.

Gustafson, A. F. 1965. *Objective Analysis of the Tropopause.* National Meteorological Center, Weather Bureau, ESSA, Washington D.C.

Newton, C. W. & Person, A. V. 1962. Structural characteristics of the subtropical jet stream and certain lower-stratospheric wind systems. *Tellus, 14,* 221–241.

Nordø, J. 1965. The vertical structure of the atmosphere. *Geophysica Norvegica, XXVI,* No. 5.

Shuman, F. G. & Hovermale, J. B. 1968. An Operational Six-Layer Primitive Equation Model. *Journal of Applied Meteorology, 7,* No. 4, 525–547.

ЭКСПЕРИМЕНТАЛЬНОЕ ИНТЕГРИРОВАНИЕ ПРИМИТИВНЫХ УРАВНЕНИЙ 4-Х УРОВЕННОЙ МОДЕЛИ АТМОСФЕРЫ

Излагется численная модель предсказания погоды. Большое внимание было уделено выбору основных уровней модели с тем, чтобы обеспечить удовлетворительное описание вертикальной структуры атмосферы. Выполнено экспериментальное интегрирование, причем в качестве начального состояния был выбран линейный бароклинный поток с малыми возмущениями. Результаты анализируются и обсуждаются со специальным ударением на процессы фронтогенеза.